

Journal of Materials Chemistry B

Accepted Manuscript



This article can be cited before page numbers have been issued, to do this please use: Q. Yang, C. Jia, Q. Chen, W. Du, Y. Wang and Q. Zhang, *J. Mater. Chem. B*, 2017, DOI: 10.1039/C6TB03193E.



This is an Accepted Manuscript, which has been through the Royal Society of Chemistry peer review process and has been accepted for publication.

Accepted Manuscripts are published online shortly after acceptance, before technical editing, formatting and proof reading. Using this free service, authors can make their results available to the community, in citable form, before we publish the edited article. We will replace this Accepted Manuscript with the edited and formatted Advance Article as soon as it is available.

You can find more information about Accepted Manuscripts in the [author guidelines](#).

Please note that technical editing may introduce minor changes to the text and/or graphics, which may alter content. The journal's standard [Terms & Conditions](#) and the ethical guidelines, outlined in our [author and reviewer resource centre](#), still apply. In no event shall the Royal Society of Chemistry be held responsible for any errors or omissions in this Accepted Manuscript or any consequences arising from the use of any information it contains.



Journal Name

ARTICLE

A NIR fluorescent probe for the detection of fluoride ions and its application for *in vivo* bioimaging

Qiuyun Yang,^a Chunman Jia,^{*ab} Qing Chen,^a Wei Du,^a Yile Wang,^a Qi Zhang^{*ab}

Received 00th January 20xx,
Accepted 00th January 20xx

DOI: 10.1039/x0xx00000x

www.rsc.org/

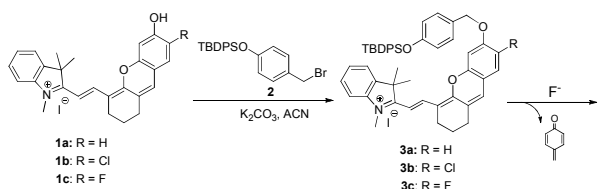
A novel near-infrared (NIR) fluorescence probe for the detection of fluoride ions has been developed, which is based on the F-triggered cleavage reaction of the Si-O bond. This probe exhibits excellent selectivity and sensitivity towards fluoride ions. The results of bioimaging experiments with *HepG2* cells and mice show that the fluoride probe is available for visualizing exogenous fluoride ions *in vitro* and *in vivo*.

Introduction

The fluoride ion, the smallest and most electronegative anion, is considered to be a micronutrient for human health that prevents dental cavities and promotes healthy bone growth.¹⁻³ Nevertheless, the toxicity of fluoride ions has also been paid much attention, since a high intake of fluoride ions could exert a great influence on the progression of distinct pathophysiological states and even lead to a diseased state.⁴⁻⁵ To achieve the complete elucidation of fluoride ion toxicity, the sensitive, specific, and accurate detection of its distribution and dynamic fluctuation in biological systems is highly desirable. Among the various analytical methods that are available, fluorescence sensing is regarded as an ideal technology due to its advantages of operational simplicity and high specificity and sensitivity. Despite remarkable advances in the development of numerous fluorescent probes of fluoride ions,⁶⁻¹⁵ there are still some drawbacks in practical applications. For example, some frequently used absorption and emission wavelengths are within the ultraviolet-visible (UV-Vis) light range, which introduces practical problems such as limited tissue penetration, high photodamage, and a low signal-to-noise ratio due to autofluorescence interference. Additionally, most reported fluorescence fluoride probes can only be applied in pure organic solvents to detect organic tetrabutylammonium fluoride rather than inorganic fluoride salts. Hence, the design of a practical fluorescence probe that responds to fluoride ions, which can be detectable in living cells and *in vivo*, is still a challenge that is essential to resolve. Over the past decade, near-infrared (NIR) fluorescent probes have become promising modalities for the bioimaging of various biologically important species, including reactive oxygen species (ROS)¹⁶⁻¹⁸ and reactive nitrogen species (RNS),¹⁹⁻²⁰ amino acids,²¹ metal ions,²²⁻²⁴ anions,²⁵⁻²⁶ enzymes²⁷ and intracellular pH changes.²⁸⁻²⁹ Compared to most other conventional fluorescent

probes, those that rely on NIR fluorescence possess unique advantages of a weaker fluorescence background, lower photodamage, intense photon penetration through deep tissues and light-scattering properties. For these reasons, recent research has been devoted to the development of NIR fluorescent probes that capable of detection and sensing of fluoride ions.³⁰ In these protocols, the classic Si-O or B-Se bond cleavage and H-F bond interaction were highly effective in response to fluoride ions, allowing the versatility of fluorescent probes with diverse NIR signaling units (e.g. DCP,³¹ BODIPY,³²⁻³³ phenanthroimidazole-cyanine,³⁴ and TDP³⁵). However, all such NIR probes have not been employed to successfully image of fluoride ions *in vivo*.

To address this issue, we proposed a hemicyanine skeleton **1** as the fluorescent report motif, which possesses NIR spectroscopic features, good photostability, and excellent water solubility. By incorporating the trigger moiety 4-(bromomethyl)phenoxy)(tert-butyl)diphenylsilane into this stable hemicyanine skeleton, we developed a turn-on NIR fluorescence probe **3** depending on the rapid cleavage reaction of a Si-O bond (Scheme 1). Further experiments disclosed that it is suitable for the real-time detection *in vivo* bioimaging of exogenous fluoride ions.



Scheme 1 The synthesis method of probe 3.

Experimental section

Materials and Instruments

All experimental reagents and materials were purchased from commercial suppliers, and dehydration acetonitrile was dried over CaH₂. Deionized water was used throughout the experiment process. UV-Vis spectrophotometer (UV-1800, Shimadzu) with 1.0 cm quartz cell was used to record the absorbance spectra. NMR

^aHainan Provincial Key Lab of Fine Chemistry, Hainan University, Haikou, Hainan 570228, China. *E-mail: zhangqi@hainu.edu.cn; jiachunman@hainu.edu.cn
Tel: +86-0898-66257271

^bKey Study Center of the National Ministry of Education for Tropical Resources Utilization, Hainan University, Haikou, Hainan 570228, China.

†Electronic Supplementary Information (ESI) available: ¹H NMR, ¹³C NMR, HRMS data of compounds 1a-c and 3a-c, pH effect of 1a-c, HPLC analysis, fluorescence imaging, UV-Vis absorption and fluorescence emission spectroscopic studies. See DOI: 10.1039/x0xx00000x

ARTICLE

Journal Name

spectra were recorded on a Bruker AVANCEII 400 MHz NMR spectrometer using TMS as the internal standard and CDCl₃ or CD₃OD as the solvent. Chemical shifts were reported in ppm from the solvent resonance as the internal standard (CDCl₃: δ_H = 7.26 ppm, δ_C = 77.16 ppm; CD₃OD: δ_H = 3.31 ppm, δ_C = 49.00 ppm). Thin layer chromatography (TLC) analysis was performed on silicagel plates (GF254, 0.20-0.25 mm). Column chromatography was conducted over a silica gel (200-300, mesh size) purchased from Qingdao Ocean Chemicals or neutral aluminium oxide (200-300, mesh size) obtained from Shanghai Macklin Biochemical Co., Ltd. The fluorescence spectra were recorded on a F97pro fluorospectrophotometer, both of the excitation and emission slit widths were setting at 10.0 nm. High resolution mass spectrum (HRMS) was determined on an LCMS-IT TOF (LC30A, Shimadzu). HPLC experiments were carried out using a C18 column (ShoaeX, 4.6 mmID×250 mL) with a LC1620A HPLC system. The mobile phase methanol was HPLC grade. Fluorescence imaging in *HepG2* cells used a laser confocal microscope (Leica TCS SP8 CARS) and *in vivo* obtained by small animal living imaging system IVIS Lumina Series III (Perkin Elmer).

General procedures of spectra detection

The stock solutions of **3a-c** (0.2 mM) were prepared in dimethyl sulfoxide (DMSO). Analytes (10 mM) were prepared in deionized water. (analytes: CH₃COONa·3H₂O, NaHCO₃, NaNO₃, NaF, Na₂CO₃, (CH₃CH₂CH₂CH₂)₄N⁺F⁻, (CH₃CH₂CH₂CH₂)₄N⁺Cl⁻, (CH₃CH₂CH₂CH₂)₄N⁺Br⁻, (CH₃CH₂CH₂CH₂)₄N⁺I⁻, NaHS, NaSCN, Na₂SO₄, NaH₂PO₄·2H₂O, Na₂S₂O₃·5H₂O, FeCl₂, KCl, MgSO₄, MnCl₂, Ni(NO₃)₂, Zn(NO₃)₂, AlCl₃, NaCl, CuCl₂, Ca(NO₃)₂). **3a-c** (10 μM, 200 μL) was placed in a 5 mL centrifugal tube, and then being diluted to 4 mL with DMSO (2.6 mL) and PBS (0.01 M, pH=7.4) (1.2 mL). Finally, the analytes were added according to the demands in the experiment process, and fluorescence emission spectra and UV-Vis absorbance spectra were recorded.

Synthesis and characterization of 1 and 3

Synthesis of compounds 1a-c

Compounds **1a-c** were synthesized according to previous report.³⁶ A mixture of compound 6 (2.0 mmol) and K₂CO₃ (276 mg, 2.0 mmol) in acetonitrile (5 mL) was stirred for 20 min at room temperature under nitrogen atmosphere. Then a solution of compound 5 (610 mg, 1.0 mmol) in acetonitrile (5 mL) was added to the above mixture via a syringe, and the reaction mixture was heated at 50 °C for 4 h. Finally the solvent was evaporated under reduced pressure, and the crude product was purified by column chromatography (CH₂Cl₂/0-30% methanol) on silica gel, affording the desired compound **1a-c** as a blue-green solid.

1a: (yield 57.4%) ¹H NMR (400 MHz, CD₃OD) δ 8.39 (d, *J* = 13.7 Hz, 1H), 7.48 (s, 2H), 7.42 – 7.35 (m, 1H), 7.32 (d, *J* = 8.6 Hz, 1H), 7.22 (d, *J* = 7.4 Hz, 2H), 6.70 (d, *J* = 7.4 Hz, 1H), 6.53 (s, 1H), 6.01 (d, *J* = 13.8 Hz, 1H), 3.57 (s, 3H), 2.69 (s, 2H), 2.62 (s, 2H), 1.87 (s, 2H), 1.72 (s, 6H). ¹³C NMR (100 MHz, CD₃OD) δ 176.04, 173.33, 163.66, 158.71, 144.48, 141.86, 140.81, 140.76, 130.99, 129.68, 125.61, 123.24, 122.62, 122.46, 116.21, 115.68, 111.26, 103.61, 99.43, 49.96, 31.33, 29.36, 28.78, 25.22, 22.02. HRMS (ESI, *m/z*) Calcd for [C₂₆H₂₆INO₂-I⁻]: 384.1958, found: 384.1928.

1b: (yield 48.5%) ¹H NMR (400 MHz, CD₃OD) δ 8.42 (d, *J* = 14.1 Hz, 1H), 7.48 (d, *J* = 6.7 Hz, 2H), 7.39 (t, *J* = 7.7 Hz, 1H), 7.33 (d, *J* = 8.8 Hz, 1H), 7.28 – 7.20 (m, 2H), 6.72 (d, *J* = 8.7 Hz, 1H), 6.56 (s, 1H), 6.05 (d, *J* = 14.1 Hz, 1H), 3.59 (s, 3H), 2.70 (s, 2H), 2.63 (s, 2H), 1.88

(s, 2H), 1.73 (s, 6H). ¹³C NMR (100 MHz, CD₃OD) δ 174.81, 173.95, 163.71, 158.50, 144.44, 142.02, 141.40, 140.37, 130.94, 129.73, 125.86, 123.29, 123.02, 121.95, 116.17, 115.80, 111.48, 103.55, 99.90, 50.15, 31.45, 29.45, 28.71, 25.24, 22.02. HRMS (ESI, *m/z*) Calcd for [C₂₆H₂₅ICINO₂-I⁻]: 418.1574, found: 418.1573.

1c: (yield 49.9%) ¹H NMR (400 MHz, CDCl₃) δ 8.08 (d, *J* = 13.4 Hz, 1H), 7.35 (s, 1H), 7.30 (s, 1H), 7.28 (s, 1H), 7.26 (d, *J* = 0.9 Hz, 1H), 7.06 (t, *J* = 7.4 Hz, 1H), 6.96 (d, *J* = 10.2 Hz, 1H), 6.85 (d, *J* = 7.8 Hz, 1H), 6.77 (d, *J* = 6.9 Hz, 1H), 5.60 (d, *J* = 13.4 Hz, 1H), 3.37 (s, 3H), 2.70 (t, *J* = 6.0 Hz, 2H), 2.63 (t, *J* = 6.5 Hz, 2H), 1.95 – 1.87 (m, 2H), 1.67 (s, 6H). ¹³C NMR (100 MHz, CDCl₃) δ 164.88, 148.39, 142.17 (d, ¹*J*_{F-C} = 245.8 Hz), 141.80, 139.75, 130.59, 127.56, 127.15, 121.43, 118.04, 113.37, 113.16, 109.19, 108.46, 103.89 (d, ²*J*_{F-C} = 17.1 Hz), 101.78, 99.58, 91.05, 53.42, 39.60, 39.29, 38.39, 37.88, 35.12, 32.53. ¹⁹F NMR (376 MHz, CDCl₃) δ -134.89. HRMS (ESI, *m/z*) Calcd for [C₂₆H₂₅IFNO₂-I⁻]: 402.1869, found: 402.1861.

Synthesis of compounds 3a-c

Compound **2** were synthesized according to the reported method.³⁷ To a stirred solution of compound **1** (0.3 mM) in acetonitrile were added K₂CO₃ (62.2 mg, 0.45 mM) and compound **2** (127.6 mg, 0.30 mM). The reaction mixture was stirred at 50 °C for 5 h under nitrogen atmosphere. The solvent was evaporated under reduced pressure, and the crude products **3** were purified by neutral aluminium oxide column chromatography using CH₂Cl₂/0-20% methanol as eluent.

3a: (yield 55.0%) ¹H NMR (400 MHz, CDCl₃) δ 8.57 (d, *J* = 14.8 Hz, 1H), 7.69 (s, 2H), 7.67 (s, 2H), 7.48 (d, *J* = 3.9 Hz, 2H), 7.45 (d, *J* = 7.4 Hz, 1H), 7.42 – 7.39 (m, 1H), 7.39 (s, 1H), 7.37 (s, 1H), 7.35 (s, 2H), 7.33 (s, 2H), 7.31 (s, 1H), 7.24 (s, 1H), 7.22 (s, 1H), 7.09 (dd, *J* = 11.5, 5.4 Hz, 3H), 6.79 (s, 1H), 6.77 (s, 1H), 6.64 (d, *J* = 14.9 Hz, 1H), 5.16 (s, 2H), 4.14 (s, 3H), 2.79 (s, 2H), 2.70 (s, 2H), 1.91 (s, 2H), 1.72 (s, 6H), 1.07 (s, 9H). ¹³C NMR (100 MHz, CDCl₃) δ 177.58, 162.16, 161.59, 155.94, 154.34, 145.76, 142.28, 141.48, 135.51, 133.74, 132.71, 130.02, 129.30, 128.92, 128.05, 127.84, 127.50, 127.28, 122.25, 120.00, 115.99, 115.28, 113.41, 112.90, 104.56, 102.01, 70.79, 50.47, 33.71, 29.71, 29.26, 28.17, 26.51, 24.38, 20.39, 19.47. HRMS (ESI, *m/z*) Calcd for [C₄₉H₅₀INO₃Si-I⁻]: 728.3554, found: 728.3499.

3b: (yield 49.9%) ¹H NMR (400 MHz, CDCl₃) δ 8.54 (d, *J* = 15.0 Hz, 1H), 7.66 (s, 2H), 7.64 (s, 2H), 7.46 (t, *J* = 8.7 Hz, 3H), 7.37 (s, 1H), 7.35 (s, 2H), 7.33 (s, 1H), 7.31 (s, 1H), 7.29 (s, 2H), 7.27 (s, 1H), 7.24 (s, 1H), 7.22 (s, 1H), 7.08 (s, 1H), 7.00 (s, 1H), 6.77 (s, 1H), 6.75 (s, 1H), 6.54 (d, *J* = 15.0 Hz, 1H), 5.17 (s, 2H), 4.06 (s, 3H), 2.71 (s, 2H), 2.66 (s, 2H), 1.85 (s, 2H), 1.71 (s, 6H), 1.05 (s, 9H). ¹³C NMR (100 MHz, CDCl₃) δ 178.01, 160.56, 156.80, 155.67, 152.59, 145.74, 142.09, 141.50, 135.38, 132.62, 131.64, 129.89, 129.20, 128.74, 128.45, 127.84, 127.71, 127.52, 122.38, 120.65, 119.85, 115.81, 115.16, 112.96, 105.03, 101.60, 71.59, 50.68, 33.98, 29.19, 27.87, 26.42, 24.30, 20.15, 19.36. HRMS (ESI, *m/z*) Calcd for [C₄₉H₄₉ICINO₃Si-I⁻]: 762.3170, found: 762.3170.

3c: (yield 53.3%) ¹H NMR (400 MHz, CDCl₃) δ 8.58 (d, *J* = 14.9 Hz, 1H), 7.69 (d, *J* = 1.3 Hz, 2H), 7.67 (d, *J* = 1.5 Hz, 2H), 7.45 (d, *J* = 5.4 Hz, 2H), 7.43 (s, 1H), 7.39 (s, 1H), 7.37 (s, 1H), 7.35 (d, *J* = 2.0 Hz, 2H), 7.33 (d, *J* = 1.2 Hz, 2H), 7.31 (d, *J* = 1.4 Hz, 1H), 7.23 (s, 1H), 7.18 (s, 1H), 7.16 (s, 1H), 6.87 (dd, *J* = 8.1, 5.3 Hz, 2H), 6.78 (s, 1H), 6.76 (s, 1H), 6.55 (d, *J* = 14.9 Hz, 1H), 5.01 (s, 2H), 4.04 (s, 3H), 2.75 (s, 2H), 2.70 (s, 2H), 1.89 (s, 2H), 1.72 (s, 6H), 1.07 (s, 9H). ¹³C NMR (100 MHz, CDCl₃) δ 177.93, 161.02, 156.03, 150.20 (d, ¹*J*_{F-C} = 245.9 Hz), 150.41, 150.28, 150.12, 148.97, 145.81, 142.38, 141.56, 135.54,

132.75, 132.30, 130.05, 129.37, 128.85, 127.87, 127.66 (d, $^2J_{F-C}$ = 36.1 Hz), 122.38, 120.04, 115.33, 115.13 (d, $^3J_{F-C}$ = 8.1 Hz), 113.08, 105.08, 103.11, 72.08, 50.69, 34.23, 29.76, 29.39, 28.06, 26.55, 24.50, 20.32, 19.51. ^{19}F NMR (376 MHz, CDCl_3): δ -134.93. HRMS (ESI, m/z) Calcd for $[\text{C}_{49}\text{H}_{49}\text{IFNO}_3\text{Si}^-]$: 746.3466, found: 746.3461.

Detection limit

The detection limit was calculated on the basis of the fluorescence titration.³⁸ The fluorescence emission spectrum of **3a-c** (10 μM) were measured 10 times in a PBS/DMSO = 3 : 7 (v/v, 0.01 M, pH = 7.4) solution, and the standard deviation of blank measurement was achieved. To gain the slope, the ratio of the emission intensity at 730-740 nm was plotted against the concentration of NaF. The detection limit was calculated using the following equation:

$$\text{Detection limit} = 3 \sigma/k,$$

Where σ is the standard deviation of blank measurement, and k is the slope between the ratio of fluorescence emission intensity versus NaF.

Photostability

The photostability of probe **3a-c** were investigated in DMSO/PBS = 7 : 3 (v/v, 0.01 M, pH = 7.4) solution, which placed in closed box with an UV lamp (254 nm) 25 cm away from the testing solutions.³⁹ Recorded their fluorescence intensity and UV absorption at different time.

HPLC experiments

HPLC experiments were carried out using a C18 column (Shoax, 4.6 mmID \times 250 mmL) with a LC1620A HPLC system. The mobile phase was a methanol. The flow rate was 0.8 mL/min and detection at 600 nm. The detection solutions of **1a-c** (0.2 mM), **3a-c** (0.2 mM) and NaF (0.0, 0.5, 1.0, 1.5 equiv., respectively) in a PBS/DMSO = 3:7 (v/v, 0.01 M, pH = 7.4) solution at room temperature.

Cytotoxicity Assay

The cytotoxicity of probe **3a-c** was determined by MTT assays.¹⁸ HepG2 cells were incubated in Dulbecco's Modified Eagle Medium (DMEM) supplemented with 10% FBS (fetal bovine serum) in an atmosphere of 5% CO_2 and 95% air at 37 $^\circ\text{C}$. The cells were placed in a 96-well plate and incubated for 24 h upon different concentrations of probe **3c** of 0.0, 5.0, 10.0, 20.0, 40.0, 60.0 and 80.0 μM , respectively. Finally, the MTT assay followed. The cytotoxic effect (VR) of probe **3c** was assessed using the following equation:

$$\text{VR} = A/A_0 \times 100\%,$$

Where A and A_0 are the absorbance of the experimental group and control group using a microplate reader at 490 nm, respectively. Probe **3a** and **3b** were also evaluated under the same condition.

Living cell culture and imaging

HepG2 Cells were cultured in Dulbecco's Modified Eagle Medium (DMEM) supplemented with 10% FBS (fetal bovine serum). Before imaging, the cells were seeded in 12-well flat-bottomed plates in an atmosphere of 5% CO_2 , 95% air at 37 $^\circ\text{C}$, and seeding at a density of about 80% - 90%. Immediately before the experiments, the cells were washed twice with PBS buffer. Subsequently, the cells were incubated with **3a-c** (20 μM) in PBS (containing 5% DMSO as a cosolvent) for 1h at 37 $^\circ\text{C}$, and then washed with PBS three times. For the experiment group, the cells were added a NaF (100 μM , 2

mL) solution for 10 min, then washed with PBS three times. The cells were stained with Hoechst for 10 min, and then washed with PBS three times. Finally the cells were fixed by paraformaldehyde (4%) 10 min at room temperature. Fluorescence imaging were then carried out after washing the cells with PBS which was conducted using a laser confocal microscope by exciting at 690 nm and emission at about 750 nm.

Living animal imaging

All animal operations were in accordance with institutional animal use and care regulations approved by the Jiangsu University laboratory animal centre. The study was performed with the Guidelines for the care and use of research animals. First, **3c** (20 μM , 192 μL) was injected into nude mouse bodies through the tail vein as a control experiment. Second, **3c** (20 μM , 192 μL) was injected into nude mouse bodies through the tail vein with a certain concentration of sodium fluoride solution by intraperitoneal injection. The amounts of sodium fluoride used were 28 mgF/kg, 12 mgF/kg, and 2 mgF/kg. The fluorescence distributions in the mice were recorded using a small animal living imaging system after gas anaesthesia at 15 min, 2 h, and 4 h.

Results and Discussion

Our probe design focused on 7-substituted **1** that differ in their pKa of the phenol group but have similar steric demands during binding. As shown in Scheme 1, hemicyanines **1a** were obtained according to the method reported by Lin *et al.*⁴⁰ Compounds **1b** and **1c** (Scheme 1), the chloro- and fluoro-substituted **1a**, respectively, were synthesized as controls to investigate the role of the halogen group in the modulation of the photophysical profiles. As the response site for the fluoride ion, a silyl group of tert-butyldiphenylsilyl (TBDPS) was attached to **1a-c** to prepare probes **3a-c**. We first investigated the absorption and emission profiles of compounds **1a-c**. As shown in Fig. 1(A), the solutions of **1a-c** (10 μM , PBS/DMSO = 3 : 7 (v/v, 0.01 M, pH = 7.4)) showed maximum absorptions at 707, 717 and 708 nm, respectively. The fluorescence intensities of **1a-c** gradually stabilized at pH 4.9, 5.4 and 6.4 (Fig. 1(B)), respectively. Their pKa values were calculated according to the Henderson-Hasselbach-type mass action equation. The pKa value of **1c** (4.1) was lower than those of **1a** (5.5) and **1b** (4.4) (Table 1), which indicates that it could be reasonably applied to biological systems, and the application of **1c** in physiological conditions is relatively extensive. The UV-Vis absorptions of **1a-c** are all stable and change negligibly when the pH is increased to 7.4 (Fig. S5, S10, S15). Thus, **3a-c** operates well in the physiological pH region, and pH 7.4 was chosen as the experimental condition.

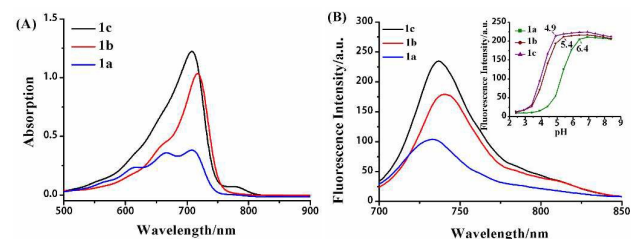


Fig. 1 (A) The UV-Vis absorption of **1a-c** (10 μM). (B) The fluorescence emission of **1a-c** (10 μM). Inset: the correlation between fluorescence emission intensity and pH (2.4-8.4). All data were measured in PBS/DMSO = 3 : 7 (v/v, 0.01 M, pH = 7.4).

Table 1 Photophysical Data of **1a-c**

	$\lambda_{\text{abs}}(\text{nm})^a$	$\lambda_{\text{em}}(\text{nm})^b$	$\epsilon_{\text{max}}(10^4 \text{ M}^{-1} \text{ cm}^{-1})^c$	Φ^d	pK_a^e
1a	707	732	3.82	0.13	5.5
1b	717	740	6.85	0.36	4.5
1c	708	736	12.24	0.41	4.1

^aMaximal absorption. ^bMaximal emission wavelength. ^cMolar extinction coefficient. ^dRelative fluorescence quantum yield estimated using indocyanine green (ICG, $\Phi = 0.13$ in DMSO) as a fluorescence standard. ^eCalculated using Henderson-Hasselbach-type mass action equation ($\log[(F_{\text{max}}-F)/(F-F_{\text{min}})]=\text{pKa}-\text{pH}$).⁴⁰ Concentrations of **1a-c** are 10 μM . Measured in PBS/DMSO = 3 : 7 (v/v, 0.01 M, pH = 7.4). $\lambda_{\text{ex}} = 690 \text{ nm}$.

Spectroscopic studies of **3a-c** towards fluoride ions

To evaluate the fluoride ion sensing ability of the system, the UV-Vis absorption and fluorescence spectra of **3a-c** (10 μM) were recorded in the presence of F^- in a PBS/DMSO = 3:7 (v/v, 0.01 M, pH = 7.4) solution at room temperature. **3c** shows a major absorption peak at 612 nm ($\epsilon_{\text{max}} = 4.76 \times 10^4 \text{ M}^{-1} \text{ cm}^{-1}$) (Table 2). When NaF (0.0, 1.0, 2.0, 3.0, 4.0, 5.0, 6.0, 7.0, 8.0, 9.0, 10.0, 11.0, 12.0 equiv.) was continually added to the solution, the absorbance at 612 nm gradually decreased and a new peak appeared at 708 nm with two isosbestic points at 479 nm and 650 nm, which demonstrates the formation of a new species. The maximum absorption peak showed a 96 nm wavelength bathochromic shift, and the colour of the solution turned from blue to green. As expected, the absorption of the new species coincided with that of **1c** (Fig. 2(A)), indicating that the cleavage of the Si-O bond was triggered by fluoride ions.

Under the same condition, **3a** shows an absorption band centred at 611 nm ($\epsilon_{\text{max}} = 4.70 \times 10^4 \text{ M}^{-1} \text{ cm}^{-1}$) (Table 2). The incremental addition of NaF led to a progressive decrease of the absorption at 611 nm, while a new absorbance band appeared at approximately 707 nm and its absorption increased, similar to the case for **1a**. Two clear isosbestic points were observed at 485 nm and 665 nm (Fig. S8). The UV-Vis absorption spectra of **3b** similarly exhibited maximum absorption at 609 nm ($\epsilon_{\text{max}} = 4.19 \times 10^4 \text{ M}^{-1} \text{ cm}^{-1}$). Upon the addition of NaF (from 0 to 12 equiv.), the absorption at 609 nm decreased noticeably and a 108 nm bathochromic shift of the absorption peak to 717 nm occurred. Two clear isosbestic points at 484 nm and 656 nm were observed, accompanied by a solution colour change from blue to green (Table 2, Fig. S13). **3c** (96 nm) and **3b** (56 nm), so they have clearer colour changes upon the addition of NaF to solutions **3a-b**.

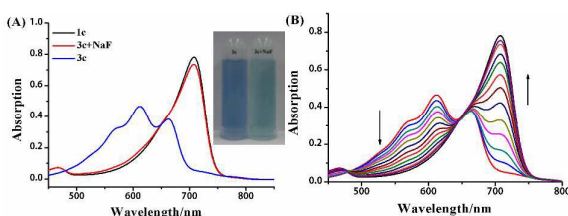


Fig. 2 (A) The UV-Vis absorptions of **1c** (10 μM), **3c** (10 μM) and **3c** (10 μM) + NaF (3.0 equiv.), measured in PBS/DMSO = 3 : 7 (v/v, 0.01 M, pH = 7.4). Inset: the colour of **3c** and **3c**+NaF. (B) UV titration of **3c** (10 μM) upon addition of NaF in a PBS/DMSO = 3 : 7 (v/v, 0.01 M, pH = 7.4) solution. Each spectrum was recorded at 10 min after the addition of NaF (0.0 - 12.0 equiv.).

Table 2 Photophysical Data of **3a-c**

	$\lambda_{\text{abs}}(\text{nm})^a$	$\lambda_{\text{em}}(\text{nm})^b$	$\epsilon_{\text{max}}(10^4 \text{ M}^{-1} \text{ cm}^{-1})^c$	$\text{DL}(\mu\text{M})^d$
3a	611	731	4.70	0.116
3b	609	739	4.19	0.061
3c	612	733	4.76	0.152

^aMaximal absorption. ^bMaximal emission wavelength after reacting with NaF. ^cMolar extinction coefficient. ^dDetection limit.⁴² Concentrations of **3a-c** are 10 μM . Measured in PBS/DMSO = 3 : 7 (v/v, 0.01 M, pH 7.4). $\lambda_{\text{ex}} = 690 \text{ nm}$.

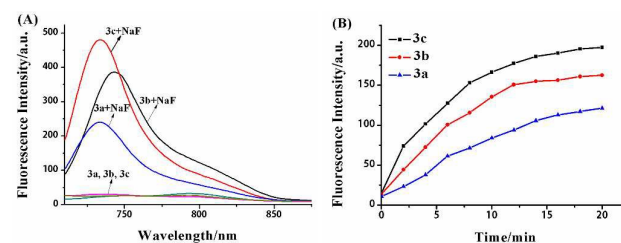


Fig. 3 (A) Fluorescence responses of **3a-c** for NaF (3.0 equiv.). (B) Time-dependent fluorescence intensity changes of **3a-c** (10 μM) upon addition of NaF (2.0 equiv.). Measured in a PBS/DMSO = 3 : 7 (v/v, 0.01 M, pH = 7.4) solution. $\lambda_{\text{ex}} = 690 \text{ nm}$.

To investigate the effect of H, Cl and F substituents on the fluorescence properties, their fluorescence emission were measured at the same conditions (PBS/DMSO = 3 : 7 (v/v, 0.01 M, pH = 7.4)). As shown in Fig. 3(A), **3a-c** all experience clear fluorescence intensity changes after NaF (3.0 equiv.) is added. Subsequently, we analysed the time-dependent fluorescence intensity changes of **3a-c** (10 μM) after the addition of NaF (2.0 equiv.). From the trends of the three lines, we found that the response of **3c** is more rapid than those of **3a-b**. The fluorescence intensities of **3c** and **3b** tended to stabilize at approximately 20 min, whereas the stabilization of **3a** was longer. The fluorescence intensity and response rate of **3c** are superior to those of the other two.

Selectivity and tolerance of **3a-c** for NaF over other analytes

For the further evaluation of the fluoride-sensing ability of the system, the selectivity and tolerance of **3a-c** for NaF over other analytes were also tested. As shown in Fig. 4(A), only NaF and TBAF demonstrated strong fluorescence emissions at 733 nm, while the other analytes ($\text{H}_2\text{PO}_4^{2-}$; Ac^- ; SO_4^{2-} ; $\text{S}_2\text{O}_3^{2-}$; HS^- ; SCN^- ; Cl^- ; Br^- ; I^- ; CO_3^{2-} ; NO_3^- ; HCO_3^- ; Cu^{2+} ; Zn^{2+} ; Mn^{2+} ; Ni^{2+} ; Mg^{2+} ; Fe^{2+} ; Ca^{2+} ; Al^{3+} ; K^+ ; Na^+) (3.0 equiv.) show almost no fluorescence response for **3c** (10 μM). This observation clearly demonstrates the high selectivity of **3c** towards F^- over other analytes. Evidently, the presence of these analytes did not have a remarkable influence on the fluorescence response process of NaF to **3c** (Fig. 4(B)). This indicates that **3c** has a great tolerance for F^- over other analytes. Although the responses of **3a** and **3b** to F^- exhibit slight decreases, they still have similar fluorescent properties and changes (Fig. S6, S7, S11, S12). This result indicates that the system is an excellent sensitive sensor for recognizing fluoride ions over other analytes.

In order to investigate the correlation between the concentration of NaF and the fluorescence intensity, a fluorescence titration experiment was then conducted. As shown

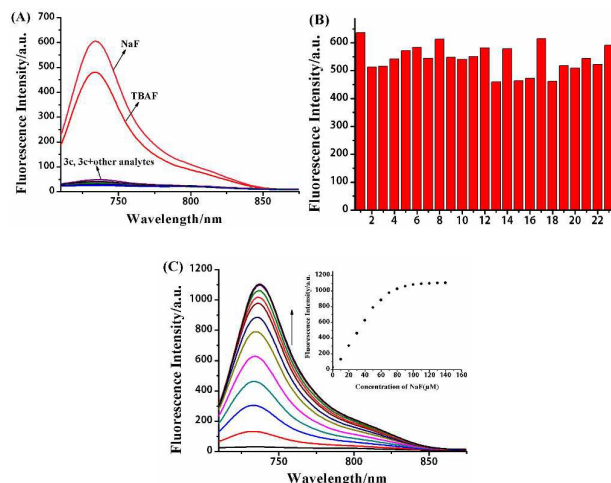


Fig. 4 (A) Fluorescence response of **3c** (10 μM) to various analytes (3.0 equiv.). Other analytes ($\text{H}_2\text{PO}_4^{2-}$; Ac^- ; SO_4^{2-} ; $\text{S}_2\text{O}_3^{2-}$; HS^- ; SCN^- ; Cl^- ; Br^- ; I^- ; CO_3^{2-} ; NO_3^- ; HCO_3^- ; Cu^{2+} ; Zn^{2+} ; Mn^{2+} ; Ni^{2+} ; Mg^{2+} ; Fe^{2+} ; Ca^{2+} ; Al^{3+} ; K^+ ; Na^+). (B) Fluorescence intensity of **3c** (10 μM) in the presence of NaF (3.0 equiv.) with other analytes (10.0 equiv.). Horizontal axis: (1) F^- ; (2) $\text{F}^- + \text{SCN}^-$; (3) $\text{F}^- + \text{HS}^-$; (4) $\text{F}^- + \text{S}_2\text{O}_3^{2-}$; (5) $\text{F}^- + \text{SO}_4^{2-}$; (6) $\text{F}^- + \text{Ac}^-$; (7) $\text{F}^- + \text{H}_2\text{PO}_4^{2-}$; (8) $\text{F}^- + \text{HCO}_3^-$; (9) $\text{F}^- + \text{NO}_3^-$; (10) $\text{F}^- + \text{I}^-$; (11) $\text{F}^- + \text{Br}^-$; (12) $\text{F}^- + \text{Cl}^-$; (13) $\text{F}^- + \text{CO}_3^{2-}$; (14) $\text{F}^- + \text{Cu}^{2+}$; (15) $\text{F}^- + \text{Zn}^{2+}$; (16) $\text{F}^- + \text{Mn}^{2+}$; (17) $\text{F}^- + \text{Ni}^{2+}$; (18) $\text{F}^- + \text{Mg}^{2+}$; (19) $\text{F}^- + \text{Fe}^{2+}$; (20) $\text{F}^- + \text{Ca}^{2+}$; (21) $\text{F}^- + \text{Al}^{3+}$; (22) $\text{F}^- + \text{K}^+$; (23) $\text{F}^- + \text{Na}^+$. (C) Fluorescence titration studies of **3c** (10 μM) upon addition of NaF (0.0 - 11.0 equiv.) at room temperature. Inset: Linear correlation between the fluorescence intensity and the concentration of NaF. Measured in a PBS/DMSO = 3: 7 (v/v, 0.01 M, pH = 7.4) solution, 10 min after the addition of NaF.

in Fig. 4(C), the fluorescence intensity is clearly increasing with the addition of NaF. As the concentration of NaF increases to 100 μM (10.0 equiv.), the fluorescence intensity reaches its maximum level, an approximately 37-fold enhancement. The fluorescence responses of **3a** and **3b** to NaF achieved their maximum levels at approximately 120 μM (Fig. S9) and 110 μM (Fig. S14), approximately 27-fold and 28-fold enhancements, respectively. From the inset diagrams of the three probes, the fluorescence intensity has an excellent linear correlation with the concentration of NaF in the range of 0 to 100 μM (probe **3a**, Fig. S9), 0 to 70 μM (probe **3b**, Fig. S14), 0 to 70 μM (probe **3c**, Fig. S16). The detection limits were calculated to be 0.152, 0.116 and 0.061 μM ($S/N = 3$) (Table 2), which indicates that the probe is highly sensitive and may be suitable for studies of NaF in living systems.

Photostability of probe 3a-c

The high photostability of fluorescence probes is highly desirable to perform long-time *in vivo*. Therefore the photostability of probe **3a-c** was evaluated by time-course fluorescence and UV absorption measurements upon sustained illumination. After exposed to UV lamp (254 nm) for different time, the fluorescence intensity of **3a-c** are almost no change. Simultaneously, the UV absorption only show a slight decrease (Fig. S2, S3, S4). From above results, we can know

that the probe **3a-c** are all exhibited good photostability, which is a critical factor for the long-time tracking and bioimaging *in vivo*.

Mechanism studies

To confirm the sensing mechanism, HPLC and ESI-MS methods were then carried out. We firstly detected the HPLC peaks of **3c** (0.2 mM)+ NaF (0.0 equiv. (Fig. 5a), 0.5 equiv. (Fig. 5b), 1.0 equiv. (Fig. 5c), respectively), **1c** (0.2 mM) (Fig. 5d), and solvent system (blank system, Fig. 5e). As shown in Fig. 5, after **3c** reacted with different equivalents of NaF, the peak at 23.385 min decreased, and a new peak at 5.300 min appeared, with a retention time that coincided exactly with that of **1c**. By contrast, **3a** (Fig. S17) and **3b** (Fig. S18) also show the identical results. Therefore, it is logical to expect that upon the addition of fluoride ions, the fluorescence colour change from blue to green reflects the extent of the fluoride-induced Si-O bond cleavage. It is noteworthy that in the HRMS spectra of **3c** with NaF (Fig. S32), a new peak was detected at $m/z = 402.1874$, which correspond to the product **1c**. These results strongly supports the supposition that the fluoride ions-triggered cleavage reaction causes the release of **1c**.

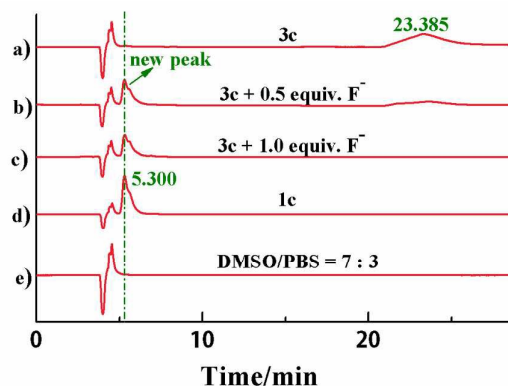


Fig. 5 HPLC chromatograms analysis, a) **3c** (0.2 mM). b) **3c** (0.2 mM)+NaF (0.5 equiv.). c) **3c** (0.2 mM)+NaF (1.0 equiv.). d) **1c** (0.2 mM). e) DMSO/PBS= 7: 3. Conditions: incubation for 10 min in a PBS/DMSO = 3 : 7 (v/v, 0.01 M, pH=7.4) solution at room temperature.

Living cell application

Based on the excellent sensing ability of probes **3a-c** to sodium fluoride in water-containing solutions, we continued to explore whether probe **3** can operate in living *HepG2* cells, and confocal fluorescence microscope images were investigated. In the control test (Fig. 6A), we cultivated cells with **3c** (20 μM) for 1 h at 37 $^{\circ}\text{C}$, and then the cell nuclei were staining with Hoechst for 10 min, displaying a blue colour by emission from the blue channel (Fig. 6a). The cells incubated with **3c** did not exhibit notable fluorescence, which indicates that none of the substances are responsive to **3c**. Meanwhile, the experimental group (Fig. 6B) was further incubated with sodium fluoride (100 μM) for another 10 min. As expected, the probe **3c** led to the enhancement of red fluorescence when the living cells loaded with **3c** were further treated with sodium fluoride, in good agreement with the fluorescence turn-on

ARTICLE

Journal Name

profile in the solution. **3a** (Fig. S22) and **3b** (Fig. S23) are similar to **3c**. These results imply that probes **3a-c** are cell membrane permeable and responsive to fluoride ions in living cells. In addition, the cytotoxicity of probe **3a-c** in living cells were also tested via MTT assay. The results indicate that the cells have low cytotoxicity upon respective treatment with **3a-c** (20 μ M) for 24 h (Fig. S19, S20, S21). This illustrates that **3a-c** possessed good biocompatibility and was suitable for biological system.

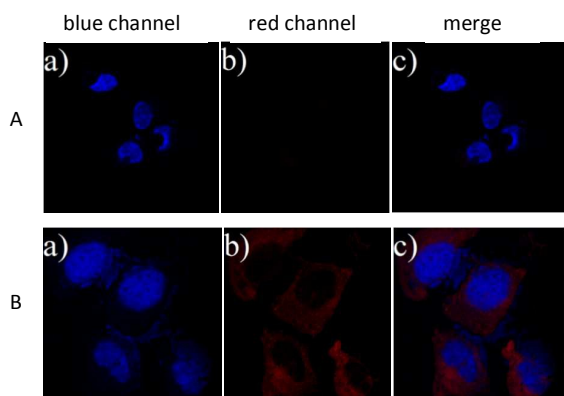


Fig. 6 Confocal microscope images of **3c** in HepG2 cells. A: control. B: Image of the cells incubated with **3c** (20 μ M) for 1 h, and further incubated with NaF (100 μ M) for 10 min. (a) emissions from the blue channel. (b) emissions from the red channel. (c) Merge.

Living animal application

The prominent features of probe **3** include NIR absorption and emission wavelengths, excellent selectivity for fluoride ions and tolerance for other analytes, good cell membrane permeability and low detection limit for sodium fluoride. These desirable attributes prompted us to further investigate the suitability of the probe for detecting fluoride ions in living animals. **3c** has more advantages than the other two and was chosen to conduct living animal imaging. First, the mice were injected with probe **3c** (20 μ M) as a control group (Fig. 7a), and then another group was treated with sodium fluoride 28 mgF/Kg (Fig. S24), 12 mgF/Kg (Fig. S25), or 2 mgF/Kg (Fig. 7) as an experiment group. The mice were anesthetized and imaged using an IVIS Lumina Series III *in vivo* imaging system. As shown in Fig. 7, the mice injected with both NaF and probe **3c** exhibit that the fluorescence intensity in the mice is time-dependent, with a maximum fluorescence intensity at 2 h, but when injected probe **3c** without sodium fluoride, they display no fluorescence (Fig. 7a). The previous studies reported that the minimum value of the human lethal fluoride dose is approximate 3 mg/Kg for children.⁴³ Gratifyingly, our probe **3c** could be utilized as an imaging probe for visualizing exogenous

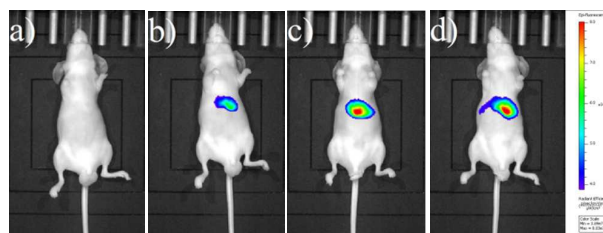


Fig. 7 Fluorescence images of **3c** in mouse. a) Mice injected with probe **3c** (20 μ M). b) Mice injected with **3c** (20 μ M) and 2 mgF/Kg sodium fluoride recorded at 15 min. c) Mice injected **3c** (20 μ M) with 2 mgF/Kg sodium fluoride recorded at 2 h. d) Mice injected **3c** (20 μ M) with 2 mgF/Kg sodium fluoride recorded at 4 h.

fluoride ions even at the level of 2 mgF/Kg body weight (Fig. 7, b-d). In order to observe the distribution of probe **3c** in the body, we analysed the anatomy in mice. From Fig. S22, we can clearly observe that probe **3c** is mainly concentrated in the liver and spleen, but not in the heart, lung or kidney.

Conclusions

In summary, we have designed and synthesized three probes **3a-c** based on hemicyanine through introducing three different substituents (F⁻, Cl⁻, and H⁻) at the ortho of the hydroxyl. We conducted pH effect, UV-titration and fluorescence titration, selective and competitive experiments. Their excitation wavelength is 690 nm and their emission wavelengths are 730-740 nm, which all belong to the NIR region. Compared with the calculated data for the UV absorption and fluorescence emission spectra, we confirmed that the fluorescence properties of **3c** have more advantages than those of the other two probes, including a faster reaction rate and stronger fluorescence intensity. HPLC and HRMS analysis verified the mechanism is based on the F⁻-triggered rapid cleavage of Si-O bond. The high specificity of probes **3a-c** for fluoride ions permits accurate detection in living biosystems. Further research of NIR probes to detect other species is underway in our laboratory, the results of which will be reported in due course.

Acknowledgements

This work has been financially supported by the National Natural Science Foundation of China (21562018, 21261008, 21166008); Natural Science Foundation of Hainan Province (20162019) for the financial assistance.

Notes and references

- 1 L. K. Kirk, *Plenum Press: New York*, 1991.
- 2 M. Kleerekoper, *Endocrinology and Metabolism Clinics of North America*, 1998, **27**, 441-452.
- 3 D. Briancon, *Rev. Rhum.*, 1997, **64**, 78.
- 4 A. L. Choi, G. Sun, Y. Zhang and P. Grandjean, *Environmental Health Perspectives*, 2012, **120**, 1362-1368.
- 5 E. T. Everett, *Journal of Dental Research*, 2011, **90**, 552-560.
- 6 Y. Zhou, J. F. Zhang and J. Yoon, *Chemical Reviews*, 2014, **114**, 5511-5571.
- 7 E. J. Cho, J. W. Moon, S. W. Ko, J. Y. Lee, S. K. Kim, J. Yoon and K. C. Nam, *Journal of the American Chemical Society*, 2003, **125**, 12376-12377.
- 8 C. Bohne, H. Ihmels, M. Waidelich and C. Yihwa, *Journal of the American Chemical Society*, 2005, **127**, 17158-17159.
- 9 C.-W. Chiu and F. P. Gabbaï, *Journal of the American Chemical Society*, 2006, **128**, 14248-14249.
- 10 X. Y. Liu, D. R. Bai and S. Wang, *Angewandte Chemie International Edition*, 2006, **45**, 5475-5478.
- 11 M. Cametti and K. Rissanen, *Chemical Communications*, 2009, 2809-2829.
- 12 G. Wei, J. Yin, X. Ma, S. Yu, D. Wei and Y. Du, *Analytica Chimica Acta*, 2011, **703**, 219-225.
- 13 B. Ke, W. Chen, N. Ni, Y. Cheng, C. Dai, H. Dinh and B. Wang, *Chemical Communications*, 2013, **49**, 2494-2496.

- 14 T. Sakamoto, D. Hasegawa and K. Fujimoto, *Chemical Communications*, 2015, **51**, 8749-8752.
- 15 B. Ke, W. Wu, L. Wei, F. Wu, G. Chen, G. He and M. Li, *Analytical Chemistry*, 2015, **87**, 9110-9113.
- 16 N. Karton-Lifshin, E. Segal, L. Omer, M. Portnoy, R. Satchi-Fainaro and D. Shabat, *Journal of the American Chemical Society*, 2011, **133**, 10960-10965.
- 17 K. Xu, S. Sun, J. Li, L. Li, M. Qiang and B. Tang, *Chemical Communications*, 2012, **48**, 684-686.
- 18 J. Zhang, C. Li, R. Zhang, F. Zhang, W. Liu, X. Liu, S. M.-Y. Lee and H. Zhang, *Chemical Communications*, 2016, **52**, 2679-2682.
- 19 J. Tian, H. Chen, L. Zhuo, Y. Xie, N. Li and B. Tang, *Chemistry – A European Journal*, 2011, **17**, 6626-6634.
- 20 F. Yu, P. Li, G. Li, G. Zhao, T. Chu and K. Han, *Journal of the American Chemical Society*, 2011, **133**, 11030-11033.
- 21 J. Yin, Y. Kwon, D. Kim, D. Lee, G. Kim, Y. Hu, J.-H. Ryu and J. Yoon, *Journal of the American Chemical Society*, 2014, **136**, 5351-5358.
- 22 X. Lu, W. Zhu, Y. Xie, X. Li, Y. Gao, F. Li and H. Tian, *Chemistry – A European Journal*, 2010, **16**, 8355-8364.
- 23 P. Li, X. Duan, Z. Chen, Y. Liu, T. Xie, L. Fang, X. Li, M. Yin and B. Tang, *Chemical Communications*, 2011, **47**, 7755-7757.
- 24 Y. Zhao, X. Lv, Y. Liu, J. Liu, Y. Zhang, H. Shi and W. Guo, *Journal of Materials Chemistry*, 2012, **22**, 11475-11478.
- 25 X. Chen, S.-W. Nam, G.-H. Kim, N. Song, Y. Jeong, I. Shin, S. K., Kim, J. Kim, S. Park and J. Yoon, *Chemical Communications*, 2010, **46**, 8953-8955.
- 26 W. Zhu, X. Huang, Z. Guo, X. Wu, H. Yu and H. Tian, *Chemical Communications*, 2012, **48**, 1784-1786.
- 27 T. Myochin, K. Hanaoka, T. Komatsu, T. Terai and T. Nagano, *Journal of the American Chemical Society*, 2012, **134**, 13730-13737.
- 28 H. Lee, W. Akers, K. Bhushan, S. Bloch, G. Sudlow, R. Tang and S. Achilefu, *Bioconjugate Chemistry*, 2011, **22**, 777-784.
- 29 J. Yin, Y. Hu and J. Yoon, *Chemical Society Reviews*, 2015, **44**, 4619-4644.
- 30 Y. Zhou, J. F. Zhang and J. Yoon, *Chemical Reviews*, 2014, **114**, 5511-5571.
- 31 J. Cao, C. Zhao and W. Zhu, *Tetrahedron Letters*, 2012, **53**, 2107-2110.
- 32 J. Cao, C. Zhao, P. Feng, Y. Zhang and W. Zhu, *RSC Advances*, 2012, **2**, 418-420.
- 33 W. Gong, R. Su, L. Li, K. Xu and B. Tang, *Chinese Science Bulletin*, 2011, **56**, 3260-3265.
- 34 T. Li, L. Yu, D. Jin, B. Chen, L. Li, L. Chen and Y. Li, *Analytical Methods*, 2013, **5**, 1612-1616.
- 35 Y. Li, M. Zheng, J. Wang, Y. Gao, B. Zhang and W. Yang, *Dyes and Pigments*, 2014, **104**, 97-101.
- 36 J. Zhang, J. Wang, J. Liu, L. Ning, X. Zhu, B. Yu, X. Liu, X. Yao and H. Zhang, *Analytical Chemistry*, 2015, **87**, 4856-4863.
- 37 G. R. Pettit, M. P. Grealish, M. K. Jung, E. Hamel, R. K. Pettit, J. C. Chapuis and J. M. Schmidt, *Journal of Medicinal Chemistry*, 2002, **45**, 2534-2542.
- 38 B. K. Datta, D. Thiyagarajan, S. Samanta, A. Ramesh and G. Das, *Organic & Biomolecular Chemistry*, 2014, **12**, 4975-4982.
- 39 L. Zheng, L. Wang, P. Wang, Q. Sun, X. Liu, X. Zhang and S. Qiu, *Tetrahedron Letters*, 2016, **57**, 932-936.
- 40 L. Yuan, W. Lin, S. Zhao, W. Gao, B. Chen, L. He and S. Zhu, *Journal of the American Chemical Society*, 2012, **134**, 13510-13523.
- 41 D. Oushiki, H. Kojima, T. Terai, M. Arita, K. Hanaoka, Y. Uran and T. Nagano, *Journal of the American Chemical Society*, 2010, **132**, 2795-2801.
- 42 Y. Qian, L. Cao, C. Jia, P. O. Boamah, Q. Yang, C. Liu, Y. Huang and Q. Zhang, *RSC Advances*, 2015, **5**, 77965-77972.
- 43 O. Barbier, L. Arreola-Mendoza and L. M. Del Razo, *Chemico-Biological Interactions*, 2010, **188**, 319-333.

A near-infrared fluorescence probe has been developed, which is available for visualizing exogenous fluoride ions *in vitro* and *in vivo*.

